

# Supercurrent in long ballistic graphene Josephson junctions

I. V. Borzenets<sup>1\*</sup>, F. Amet<sup>2</sup>, C. T. Ke<sup>3</sup>, K. Watanabe<sup>4</sup>, T. Taniguchi<sup>4</sup>, M. Yamamoto,<sup>1,5</sup> S. Tarucha<sup>1,6</sup>, G Finkelstein<sup>3</sup>

<sup>1</sup>Department of Applied Physics, University of Tokyo, Bunkyo-ku, Tokyo 113-8656, Japan

<sup>2</sup>Department of Physics and Astronomy, Appalachian State University, Boone, NC 28607, USA.

<sup>3</sup>Department of Physics, Duke University, Durham, NC 27708, USA.

<sup>4</sup>Advanced Materials Laboratory, National Institute for Materials Science, Tsukuba, 305-0044, Japan.

<sup>5</sup>PRESTO, JST, Kawaguchi-shi, Saitama 332-0012, Japan

<sup>6</sup>Center for Emergent Matter Science (CEMS), RIKEN, Wako-shi, Saitama 351-0198, Japan

\*Correspondence should be sent to I.V.B. (email: ivan@meso.t.u-tokyo.ac.jp)

We investigate the critical current  $I_C$  in Josephson junctions made of encapsulated graphene/boron-nitride heterostructures.  $I_C$  is found to scale with temperature  $T$  as  $\propto e^{-k_B T/\delta E}$ , which is consistent with the conventional model for ballistic Josephson junctions that are long compared to the thermal length. The extracted energy  $\delta E$  is independent of the carrier density and consistent with the level spacing of the ballistic cavity, as determined from Fabry-Perot oscillations of the junction normal resistance. However,  $\delta E$  is 2 to 2.5 times smaller than the value naively expected from the junction length. Finally, we find that at the lowest temperature,  $I_C$  saturates at a universal level determined by the product of  $\delta E$  and the number of modes across the junction width.

PACS numbers: 74.45.+c, 72.80.Vp, 74.50.+r, 73.23.-b

Encapsulated graphene/boron-nitride heterostructures emerged in the past year as a medium of choice for studying proximity-induced superconductivity in the ultra-clean limit [1–4]. These junctions support the ballistic propagation of superconducting currents across micron-scale graphene channels, and their critical current is gate-tunable across several orders of magnitude. In these devices, a rich phenomenology arises from the interplay of superconductivity with ballistic transport [1], cyclotron motion [2], and even the quantum Hall effect at high magnetic field [4]. However, the nature of the zero-field supercurrent in the long ballistic graphene Josephson junctions has so far not been investigated in sufficient detail.

Ballistic superconductor - normal metal - superconductor (SNS) junctions are characterized as “long” if the length of the normal region  $L$  is larger than the induced coherence length in the normal metal,  $\xi = \hbar v_F / \Delta$  [5–7]. Here,  $\Delta$  is the superconducting energy gap, and  $v_F$  is the Fermi velocity in the normal region. The lithographic constraints place many graphene devices in the regime  $L \gtrsim \xi$ . In the temperature range  $\delta E \ll k_B T \ll \Delta$ , where  $\delta E = \frac{\hbar v_F}{2\pi L} = \frac{\xi\Delta}{2\pi L}$ , the thermal averaging yields an exponential decay of the critical current:  $I_C \propto \exp(-k_B T/\delta E)$ . Note that  $\delta E$  is only dependent on the junction length  $L$ , and does not vary with the carrier density or the mobility (as long as the junction remains ballistic.) In this work, we demonstrate this exponential scaling and explore its dependence on the carrier density and the sample dimensions.

Our graphene layers are exfoliated from Kish graphite and encapsulated in hexagonal Boron-Nitride (hBN) using the “pick-up” method [8]. Heating at 250°C causes bubbles of trapped adsorbates to migrate towards the edges of the graphene mesa, effectively cleaning it. The edges of the graphene flake are exposed by etching

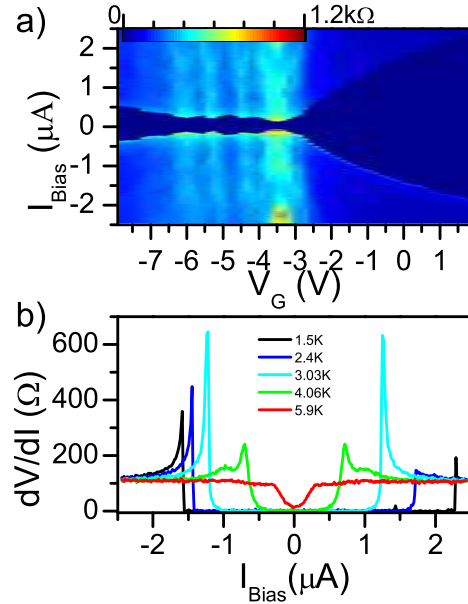


FIG. 1. a) Map of differential resistance versus current  $I$  and gate voltage  $V_G$ . The data are shown for Junction 1 and taken at a temperature  $T = 1.5K$ . The superconducting region of zero resistance can be observed around  $I = 0$ . The current through the junction is swept from negative to positive; therefore, the transition at the negative  $I$  corresponds to the retrapping current  $I_R$ , while the transition at the positive  $I$  corresponds to the switching current  $I_S$ . b) Differential resistance versus current  $I$  of Junction 1 taken at  $V_G = 1V$  for different values of temperature.

through the hBN-graphene-hBN stack with a CHF<sub>3</sub>/O<sub>2</sub> plasma (flow rates 40/6 sccm) at 1Pa and 60W power. The etching time varies depending on the thickness of the top hBN layer. We use DC magnetron sputtering to

form Molybdenum-Rhenium alloy contacts (50/50 wt%). These contacts are 100 – 120 nm thick and are deposited at a rate of  $\sim 50$  nm/min (with a pressure of 2 mTorr and a power of 160W [4].) This work presents data collected on three devices of varying width  $W$  and length  $L$ : Junction 1 ( $L = 300$  nm,  $W = 2.4\mu\text{m}$ ), Junction 2 ( $L = 800$  nm,  $W = 2.4\mu\text{m}$ ), and Junction 3 ( $L = 650$  nm,  $W = 4.5\mu\text{m}$ .)

The junctions are measured in a four-terminal lock-in setup with an AC excitation current of 5 nA added on top of a variable DC bias current,  $I$ . The carrier density in graphene is controlled with a gate voltage  $V_G$ . Figure 1A presents a map of the differential resistance  $dV/dI(V_G, I)$ , measured on Junction 1 at  $T = 1.5$  K. A supercurrent can be seen as the dark region which persists at all values of  $V_G$ . Experimentally, the current is swept from the negative to the positive values, and the transition from the normal to the superconducting state is seen in the negative region at  $|I| = I_R$  (the retrapping current.) The transition from the superconducting back to the normal state happens in the positive region when  $I = I_S$  (the switching current)[9]. As commonly observed in graphene Josephson junctions, the sample exhibits hysteresis,  $I_S \gtrsim I_R$  [10–16], which could be attributed to either underdamped junction dynamics [9, 14], or to the self-heating by the retrapping current [16, 17]. Figure 1b shows the differential resistance of Junction 1 versus bias current  $I$  taken at  $V_G = 1$  V for different temperatures. Clearly, the difference between  $I_S$  and  $I_R$  rapidly decreases with temperature, which allows to use  $I_S$  in place of the true critical current,  $I_C$ .

One can see from Figure 1b that  $I_C$  rapidly decreases with temperature. Figure 2 shows  $I_C(T)$  for devices 1 and 3 plotted on a semi-log scale for several values of  $V_G$ . From here on, the gate voltage  $V_G$  is shown relative to the Dirac point. One can see that  $\log(I_C)$  is linear in  $T$  over an order of magnitude [5–7], before saturating at both low and high temperatures. The slope of  $\log(I_C)$  does not depend on  $V_G$ , although its value increases with the device length  $L$ . Fitting a linear dependence of  $\log(I_C)$  on  $T$  yields the energy scale  $\delta E$ . We show two fitted curves for each junction on Figure 2 as a guide to the eye. The exponential dependence is particularly clear for the top curve in Fig. 2b, which shows the critical current ranging over more than two orders of magnitude. This temperature dependence strikingly differs from the short-junction regime observed in vertical graphene junctions, where  $I_C$  scales as  $\tanh(\Delta/2k_B T)$  [6, 9, 18, 19], (with  $\Delta \gg \delta E$ ). The exponential dependence is limited at the low temperature end, when  $k_B T$  becomes comparable to  $\delta E$ . Indeed, the saturation is visible in Fig. 2 at  $T \sim 1$  K for the shortest Junction 1, but not yet for Junction 3. In a separate cooldown, we have observed  $I_C$  saturating at lower temperatures in the longer Junctions 2 and 3.

The extracted energy  $\delta E$  is of the order of 0.1 meV for junction 3 and 0.15 - 0.2 meV for junction 1. Figure 3a

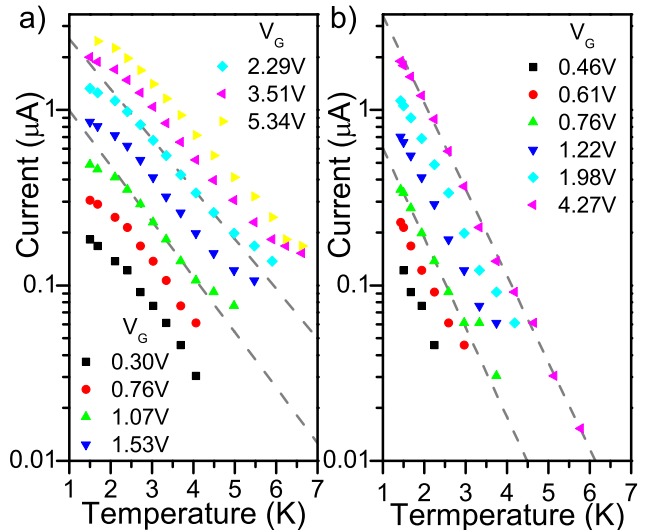


FIG. 2. Critical current  $I_C$  plotted on a semi-log scale versus temperature  $T$  for a) Junction 1 and b) Junction 3. (The values of  $V_G$  are shown relative to the Dirac point.) For a given junction, the slope of  $\log(I_C)$  vs.  $T$  is independent of the gate voltage  $V_G$ . Example fits to this exponential dependence are shown as gray dashed lines. According to theory of long ballistic SNS junctions, the slope depends on the energy  $\delta E$  which is independent of density and is inversely proportional to the junction length  $L$ . Indeed, the longer Junction 3 exhibits a steeper slope compared to the shorter Junction 1.

shows that for a given device  $\delta E(V_G)$  remains roughly constant as a function of  $V_G$  across both the electron and hole-doped regimes. Such universal scaling not dependent on carrier concentration is indeed expected in the long ballistic regime. Note, however, that the energy scale  $\delta E$  is  $\sim 2 - 2.5$  times smaller than the value  $\frac{\hbar v_F}{2\pi L}$  naively expected from the length of the device. This observation cannot be attributed to a finite reflection at superconductor-graphene interface. Indeed, the fitted energy  $\delta E$  remains largely unchanged whether the carriers are electrons or holes, while the transmission coefficient is both carrier type- and gate-dependent.

Instead, the likely explanation involves the fact that in our junctions the length is comparable with  $\xi \approx 500$  nm, and  $L$  in the definition of  $\delta E$  should be replaced with  $L + \xi$  [20]. Numerical simulations conducted in the regime  $L \approx \xi$  indicate  $I_C \propto \exp(-k_B T/\delta E)$  dependence with  $\delta E$  suppressed by a factor of  $\sim 2$  (Figure 3 in Ref. 21). Deriving a universal expression for  $\delta E$  in the  $L \approx \xi$  regime remains a theoretical challenge beyond the scope of this paper.

Remarkably, ballistic graphene Josephson junctions offer a possibility to compare  $\delta E$  to the measured level spacing in the junction,  $E_0 = \frac{\pi \hbar v_F}{L} = 2\pi^2 \delta E$ . In the hole-doped regime, the reflections of ballistic charge carriers between each contact interface yields quantum in-

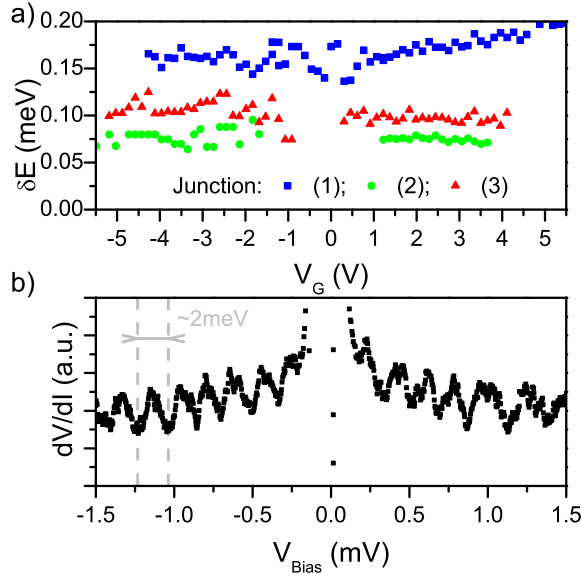


FIG. 3. (a) The gate voltage dependence of energy  $\delta E$  extracted from the slope of  $\log(I_C)$  dependence on  $T$ . Blue  $\square$  corresponds to Junction 1, green  $\circ$  to Junction 2, and red  $\triangle$  to Junction 3. As expected, the extracted energy  $\delta E$  is largely independent of  $V_G$ , regardless of whether the conduction is mediated by electrons or holes. (b) Differential conductance versus bias voltage  $V_B$  for Junction 3, gated to the p-doped regime  $V_G = -4.2V$ . The period of these oscillations should be described by the level spacing:  $E_0 = \pi\hbar v_F/L$ . The extracted value of  $\delta E \approx 2 \text{ meV}$  is consistent with the expected  $E_0 = 2\pi^2\delta E \approx 20\delta E$ .

terference (“Fabry-Perot”) oscillations in differential resistance  $dV/dI$  vs. bias voltage  $V$  with a period of  $E_0/e$  [2, 4, 22–24]. These oscillations are shown in Figure 3b for Junction 3 in the hole-doped regime. The oscillations have a period of approximately 2mV, which is in excellent agreement with  $\delta E \approx 100 \mu\text{eV}$  found from the  $I_C(T)$  fitting.

The critical current saturates in the zero-temperature limit, which is achieved when  $k_B T \ll \delta E$ . In this regime,  $I_C$  should be proportional to  $\delta E$ :  $I_C = C N e \delta E / h$ , with  $C$  being a proportionality constant. Here,  $N = W(4\sqrt{n/\pi})$  represents the number of transversal modes across the width  $W$  of the junction,  $n$  is the carrier density, and the factor 4 comes from the spin and valley degeneracies in graphene. Figure 4 shows the ratio  $\frac{hI_C}{Ne\delta E}$  as a function of gate voltage for the electron doping, when the graphene-MoRe interfaces are highly transparent [26]. Strikingly, the curves for all three junctions are very close to each other, which strongly suggests that  $\delta E$  is the relevant energy scale even as  $T \rightarrow 0$ .

Additionally, while the ratio  $\frac{hI_C}{Ne\delta E}$  is significantly reduced close to charge neutrality, it converges towards a constant (C of the order of 1) at high gate voltage. A critical current of the order of  $e\delta E/h$  per transversal mode is indeed expected in the zero temperature limit[27]. The

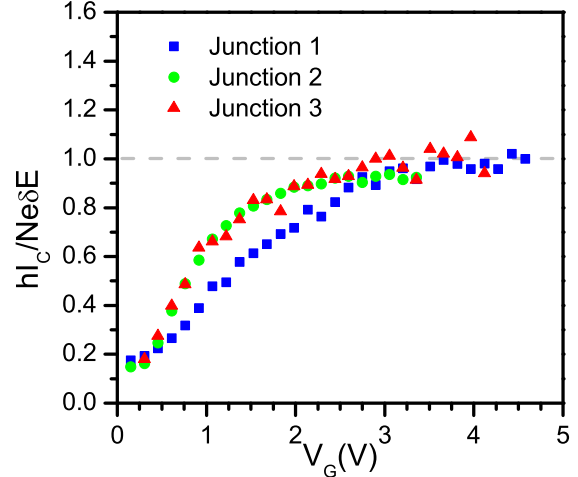


FIG. 4. Ratio  $hI_C/Ne\delta E$  as a function of  $V_G$  for junctions J1, J2 and J3, measured at 40mK. The number of modes  $N$  is  $W(4\sqrt{n/\pi})$ , where  $n$  is the carrier density as determined from  $V_G$ . Remarkably, the plotted ratio converges toward 1 in every sample as the gate voltage increases and the transmission of the graphene-MoRe interfaces gets closer to one.

suppression of  $C$  close to the Dirac point most likely arises from the  $V_G$  dependence of the transmission coefficient  $\tau$  of the superconductor-graphene interface. We extract the contact transparency from the junction normal resistance as  $h/Ne^2R_N$  and find that  $\tau$  is minimal at the charge neutrality, but gets close to 1 at high densities. Accounting for  $\tau$  [7, 25] makes the ratio  $\frac{1}{\tau^2} \frac{hI_C}{Ne\delta E}$  constant across a wider range of  $V_G$  [28].

In conclusion, we studied the nature of the critical current in several ballistic superconductor-graphene-superconductor junctions. We observed that the critical current  $I_C$  scales with temperature as  $\propto e^{-k_B T/\delta E}$ . Such behavior places the samples in the long ballistic junction regime. From the slope of  $\log I_C$  vs.  $T$  dependence, we extract the relevant energy parameter  $\delta E$ , which depends only on the junction length and is independent of the gate voltage  $V_G$ . The energy  $\delta E$  is 2 - 2.5 times smaller than the values naively extracted from the junction lengths, indicating the importance of the finite-length corrections. Finally, we show that at the lowest temperature,  $I_C$  saturates at a universal level determined by the product of  $\delta E$  and the number of transversal modes across the junction width. Our observations demonstrate the universality of the critical current in long ballistic Josephson junctions – a regime relevant to most hybrid superconductor-encapsulated graphene devices.

I. V. B. and M. Y. acknowledge the Canon foundation. C.-T. K. and G.F. were supported by the Division of Materials Sciences and Engineering, Office of Basic Energy Sciences, U.S. Department of Energy, under Award desc 0002765. F.A. acknowledges the ARO under Award

W911NF-14-1-0349. M.Y. acknowledges financial support by Grant-in-Aid for Scientific Research on Innovative Areas "Science of Atomic Layers". M. Y. and S. T. acknowledge support by Grant-in-Aid for Scientific Research S (No. 26220710), and Grant-in-Aid for Scientific Research A (No. 26247050). We would like to thank Konstantin Matveev for fruitful discussions.

---

[1] V. E. Calado, S. Goswami, G. Nanda, M. Diez, A. R. Akhmerov, K. Watanabe, T. Taniguchi, T. M. Klapwijk, and L. M. K. Vandersypen, *Nature Nano.* **10**, 761-764 (2015).

[2] M. Ben Shalom, M. J. Zhu, V. I. Fal'ko, A. Mishchenko, A. V. Kretinin, K. S. Novoselov, C. R. Woods, K. Watanabe, T. Taniguchi, A. K. Geim, and J. R. Prance, *Nature Phys.*, doi:10.1038/nphys3592 (2015.)

[3] M. T. Allen, O. Shtanko, I. C. Fulga, J. I. J. Wang, D. Nurgaliev, K. Watanabe, T. Taniguchi, A. R. Akhmerov, P. Jarillo-Herrero, L. S. Levitov, and A. Yacoby, *Nature Phys.* **12**, 128-133 (2016).

[4] F. Amet, C. T. Ke, I. V. Borzenets, Y. Wang, K. Watanabe, T. Taniguchi, R. S. Deacon, M. Yamamoto, Y. Bomze, S. Tarucha, and Finkelstein, arXiv:1512.09083 (2015).

[5] I.O. Kulik, *Sov. Phys. JETP* **30**, 944 (1970).

[6] A. V. Svidzinskii, *Spacially-Inhomogeneous Problems of Theory of Superconductivity* (Nauka, Moscow, 1982).

[7] A. A. Golubov, M. Yu. Kupriyanov, and E. Iliichev, *Rev. Mod. Phys.* **76**, 411 (2004).

[8] L. Wang, I. Meric, P. Y. Huang, Q. Gao, Y. Gao, H. Tran, T. Taniguchi, K. Watanabe, L. M. Campos, D. A. Muller, J. Guo, P. Kim, J. Hone, K. L. Shepard, and C. R. Dean, *Science* **342**, 614-617 (2014).

[9] M. Tinkham, *Introduction To Superconductivity* (McGraw-Hill, New York, 1996).

[10] H. B. Heersche, P. Jarillo-Herrero, J. B. Oostinga, L. M. K. Vandersypen, and A. F. Morpurgo, *Nature* **446**, 56 (2007).

[11] F. Miao, S. Wijeratne, Y. Zhang, U. C. Coskun, W. Bao, and C. N. Lau, *Science* **446**, 1530 (2007).

[12] X. Du, I. Skachko, and E. Y. Andrei, *Phys. Rev. B* **77**, 184507 (2007).

[13] C. Ojeda-Aristizabal, M. Ferrier, S. Guéron, and H. Bouchiat, *Phys. Rev. B* **79**, 165436 (2009).

[14] I. V. Borzenets, U. C. Coskun, S. J. Jones, and G. Finkelstein, *Phys. Rev. Lett.* **107**, 137005 (2011).

[15] I. V. Borzenets, U. C. Coskun, S. J. Jones, and G. Finkelstein, *IEEE Trans. Appl. Supercond.* **22**, 1800104 (2012).

[16] I.V. Borzenets, U.C. Coskun, H.T. Mebrahtu, Yu.V. Bomze, A.I. Smirnov, and G. Finkelstein, *Phys. Rev. Lett.* **111**, 027001 (2013).

[17] H. Courtois, M. Meschke, J. T. Peltonen, and J. P. Pekola, *Phys. Rev. Lett.* **101**, 067002 (2008).

[18] M. Titov and C. W. J. Beenakker, *Phys. Rev. B* **74**, 041401(R) (2006).

[19] G.-H. Lee, S. Kim, S.-H. Jhi, and H.-J. Lee, *Nature Commun.* **6**, 6181 (2015).

[20] P. F. Bagwell, *Phys. Rev. B* **46**, 12573-12586 (1992).

[21] I. Hagymasi, A. Kormanyos, and J. Cserti, *Phys. Rev. B* **82**, 134516 (2010).

[22] V. Cheianov and V. I. Falko, *Phys. Rev. B* **74**, 041403 (2006).

[23] F. Miao, S. Wijeratne, Y. Zhang, U. C. Coskun, W. Bao, and C. N. Lau, *Science* **317**, 15301533 (2007).

[24] P. Rickhaus, R. Maurand, M.-H. Liu, M. Weiss, K. Richter, and C. Schnenberger, *Nature Commun.* **4**, 2342 (2013).

[25] M. Yu. Kuprianov and V. F. Lukichev, *Zh. Eksp. Teor. Fiz.* **94**, 139-149 (1988).

[26] The carrier density is calculated as  $n = V_G C_G/e$  is the carrier density.  $C_G \approx 11.5nF$  is the gate capacitance. And  $V_G$  is counted from the Dirac point which is assumed to be the point where  $R_N$  is highest.

[27] C. Ishii, *Prog. Theor. Phys.* **44**, 1525 (1970).

[28] See Supplementary Information

[29] Y. Luh, *Acta Phys. Sin.* **21**, 75 (1965); H. Shiba, *Prog. Theor. Phys.* **40**, 435 (1968); A. I. Rusinov, *Sov. Phys. JETP* **29**, 1101 (1969).

# Supplementary Information

## TRANSMISSION COEFFICIENT $\tau$ AND IDEAL RESISTANCE $R_{SH}$ V.S. MEASURED $R_N$

For a device governed by ballistic transport the semiclassical limit of resistance, known as the Sharvin resistance  $R_{SH}$ , is simply the inverse of the conductance through  $N$  ballistic channels, each contributing a conductivity of  $e^2/h$ ; i.e.:  $1/R_{SH} = Ne^2/h$ . We calculate the number of modes  $N$  for each value of gate  $V_G$ :  $N = W(4\sqrt{n}/\pi)$ . Where  $n = V_G C_G/e$  is the carrier density; with  $C_G \approx 11.5 nF$  being the gate capacitance. (The factor 4 accounts for spin and valley degeneracy in graphene.)

However, the transmission across the superconductor-graphene contact interface is not unity. Therefore, the measured resistance  $R_N$  (Figure S1a) is enhanced compared to  $R_{SH}$ . The transmission coefficient of the contact interface  $\tau$  can be found by comparing the measured resistance  $R_N$  to the semiclassical limit:  $\tau = R_{SH}/R_N$ . Taking the peak of measured resistance  $R_N$  as the Dirac point, we calculate the expected  $R_{SH}$  and extract a possible transmission coefficient  $\tau$  for all three Junctions. Remarkably,  $\tau$  is fairly uniform away from the Dirac point ( $V_G > 2V$ ) and reaches values of up to 0.9 (Figure S1b).

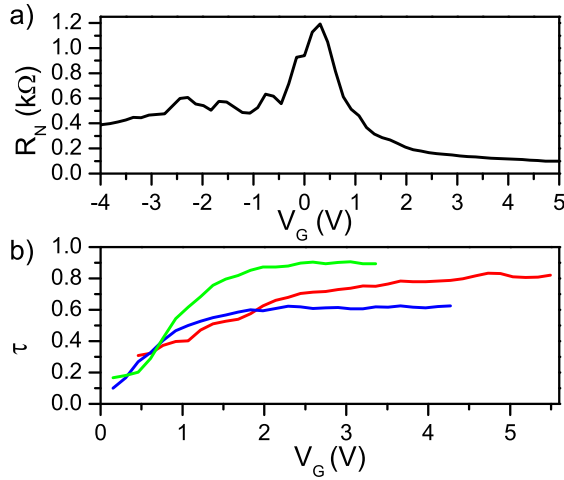


FIG. S1. a) Measured normal resistance  $R_N$  versus gate voltage  $V_G$  of Junction 1. b) Transmission coefficient of the superconductor-graphene interface  $\tau$  for Junctions 1:(blue); 2:(green); 3:(red).  $\tau$  is calculated by comparing the measured resistance to the semiclassical limit:  $\tau = R_{SH}/R_N$ ; with  $1/R_{SH} = Ne^2/h$  i.e.: the resistance of  $N$  ballistic channels.

## THE EFFECT OF $\tau$ ON THE $I_C$ V.S. $\delta E$ RELATIONSHIPS AT LOW $T$

The discussion in the main manuscript considers only the ideal long, ballistic, SNS Josephson junction in calculating the proportionality constant between  $I_C$  and  $\delta E$  at low temperatures (Figure 4). However, as the transmission across the superconductor-graphene interface is not perfect ( $\tau < 1$ ), a real junction effectively behaves as a superconductor-insulator-normal (SINIS) junction[7, 25]. For such junctions, the expected critical current is modified by the transmission. Moreover, the real resistance  $R_N$  must be used in the calculation, instead of the ideal case of  $N$  ballistic channels: effectively adding another factor of  $\tau$ . In Figure S2 we plot the ratio of  $eI_C R_N/\tau\delta E$ ; i.e.:  $\frac{1}{\tau^2} \frac{hI_C}{Ne\delta E}$ . Here we observe that the ratio saturates and becomes constant at gate voltages much closer to the Dirac point. However, the resulting ratio now varies slightly between devices:  $\sim 1.16, 1.95, 1.5$  for Junctions 1,2, and 3 respectively. Such variation could originate from an incorrect choice of the location of the Dirac point when calculating  $\tau$ . Alternatively, the variation of proportionality can come from impurities located in the graphene crystal. In a junction of finite length  $L$  single point impurities can couple to the Andreev energy levels, opening gaps in the quasiparticle level spectrum[20], without affecting the measurement of  $R_N$ . Note that Ref.20 is a general consideration of impurities in a ballistic channel: only considering the local scattering probability. Therefore, we are not able to infer anything about the nature of the impurities, such as the formation of Shiba states[29].

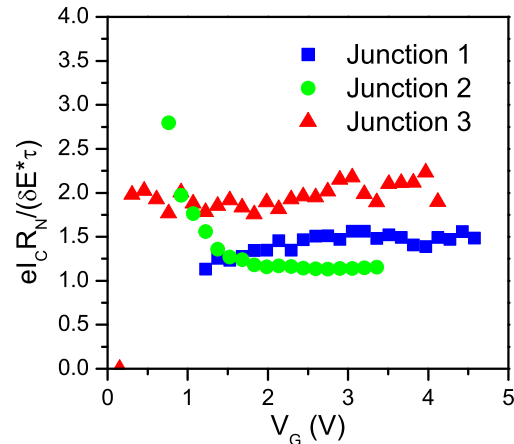


FIG. S2. The ratio  $eI_C R_N / (\tau \delta E)$  for Junction 1 (blue  $\square$ ), 2 (green  $\circ$ ), 3 (red  $\triangle$ ). The resulting ratio is gate independent with the proportionality constant  $C \sim 1$

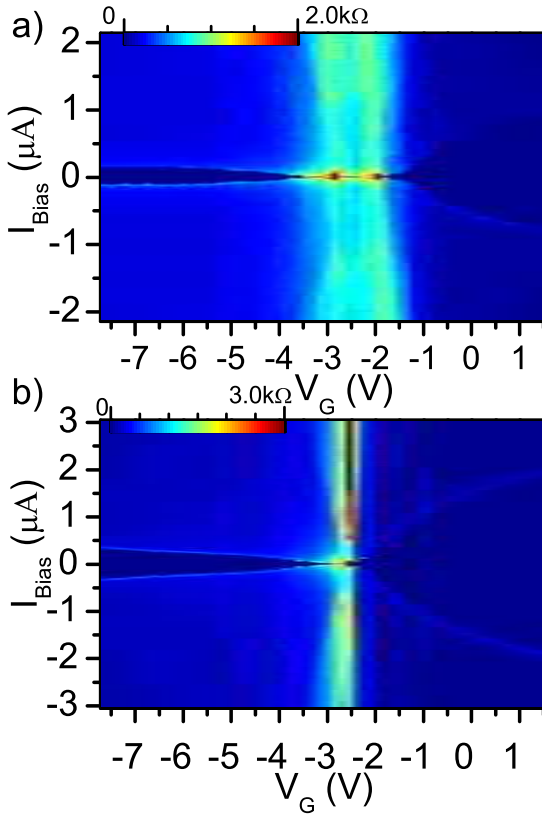


FIG. S3. Map of differential resistance versus bias current  $I$  and gate voltage  $V_G$ . The data are shown for Junction 2 (a) and Junction 3 (b) taken at a temperature  $T = 1.5K$ . The superconducting region of zero resistance can be observed around  $I = 0$ . The current through the junction is swept from negative to positive; therefore, the transition at negative  $I$  corresponds to the retrapping current  $I_R$ , while the transition at positive  $I$  corresponds to the switching current  $I_S$ .

#### DIFFERENTIAL RESISTANCE $dV/dI(V_G, I)$ JUNCTIONS 2 AND 3

Figure S3 shows maps of differential conductance versus bias current and gate voltage taken at base temperature for Junction 2 and Junction 3. Both Junction 2 and 3 are significantly longer than Junction 1, hence, oscillations in the critical current  $I_C$  in the hole conduction regime are difficult to observe. Junction 2, the longest junction, features a double peak suggesting that impurities begin to play a higher role.

#### CRITICAL CURRENT $I_C$ V.S. $T$ DEPENDENCE OF JUNCTION 2

We analyze Junction 2 in the manner identical to that of Junction 1 and 3. Figure S4 shows  $I_C(T)$  plotted on a semi-log scale for several values of  $V_G$ . (The gate voltage  $V_G$  is shown relative to the right-most Dirac peak.) Here too,  $\log(I_C)$  is linear in  $T$  up to an order of magnitude, and does not show a dependence on  $V_G$ . As Junction 2 is the longest, the slope of  $\log(I_C)$  is the highest among the three devices resulting in the lowest measurable temperature range. Fitting a linear slope to  $\log(I_C)$  yields the energy scale  $\delta E$  (Figure 3).

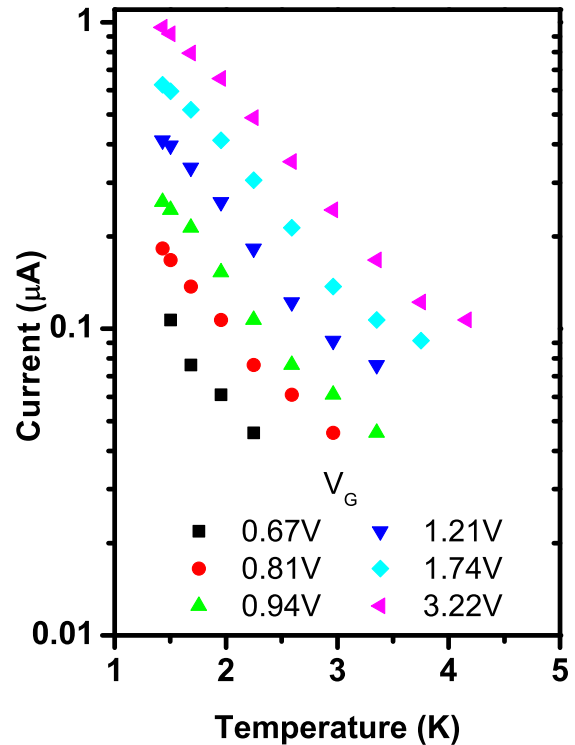


FIG. S4. Critical current  $I_C$  versus temperature  $T$  plotted on a semi-log scale for Junction 2. ( $V_G$  is shown relative to the Dirac point.) Slope of  $\log(I_C)$  v.s.  $T$  is independent of gate voltage  $V_G$ .